K-shell ionization cross sections for Si, P, K, Ca, Zn, and Ga by protons and carbon ions in the energy range 1–6.4 MeV

M. Geretschläger
Institut für Experimentalphysik, Johannes-Kepler-Universität Linz, A-4040 Linz, Austria

Ž. Šmit
J. Stefan Institute, E. Kardelj-University, Ljubljana, Yugoslavia

O. Benka
Institut für Experimentalphysik, Johannes-Kepler-Universität Linz, A-4040 Linz, Austria
(Received 6 February 1989; revised manuscript received 11 August 1989)

Absolute K-shell ionization cross sections have been measured for thin targets of Si, P, S, K, Ca, Zn, and Ga using carbon ions between 1.0 and 6.4 MeV and protons of 1 and 2 MeV. The dependence of x-ray production cross sections on target thickness was determined. The experimental results are compared to the semiclassical approximation [Laegsgaard, Andersen, and Lund in *Proceedings of the Tenth International Conference on the Physics of Electron and Atomic Collisions, Paris, 1977,* edited by G. Watel (North-Holland, Amsterdam 1977)], to the theory for direct Coulomb ionization of the $1s\sigma$ molecular orbital [Montenegro and Sigaud, J. Phys. B. **18**, 299 (1985)], to the perturbed stationary-state approximation with energy-loss, Coulomb, and relativistic corrections (ECPSSR) [Brandt and Lapicki, Phys. Rev. A **23**, 1717 (1981)], and to the modification of the ECPSSR approximation (MECPSSR) [Benka, Geretschläger, and Paul, J. Phys. (Paris) Suppl. **12**, C9-251 (1987)]. The results for carbon ions are also compared to the statistical molecular orbital theory of inner-shell ionization for symmetric or nearly symmetric atomic collisions [Mittelman and Wilets, Phys. Rev. **154**, 12 (1967)]. The proton results agree with empirical reference cross sections [Paul, Nucl. Instrum. Methods **169**, 249 (1980)]. Also, MECPSSR and ECPSSR provide best overall agreement for protons. For carbon ions the MECPSSR theory predicts the experimental data best. For the lightest targets, however, the MECPSSR underestimates the measured ionization cross sections appreciably for scaled velocities $0.4 \leq \xi \leq 0.8$. We found that in this ξ range Pauli excitation via interacting level crossing contributes strongly to the measured ionization cross section. The sum of Mittelman-Wilets predictions and MECPSSR predictions then reproduces the measured cross sections satisfactorily. This result indicates that the direct Coulomb ionization of atomic orbitals, the Pauli excitation, and the direct Coulomb ionization again, but now of molecular orbitals, are the significant K-shell ionization mechanisms for carbon ions (atomic number $Z_1 = 6$) on targets (atomic number Z_2) with $Z_1/Z_2 \sim 0.4$, for high ion velocities, intermediate velocities, and the lowest velocities, respectively.

I. INTRODUCTION

K-shell ionization studies can be classified, according to Madison and Merzbacher,[1] into two categories depending on the ratio of projectile and target atomic number (Z_1/Z_2) and on the ratio of projectile and target K-electron velocity (v_1/v_{2K}). In symmetric or near-symmetric collision systems where $Z_1/Z_2 \sim 1$, electron promotion in the transiently formed quasimolecule is the primary ionization process for $v_1 \ll v_{2K}$. Wille and Hippler[2] distinguish among three types of quasimolecular excitation mechanisms:

(i) promotion of electrons into the continuum;

(ii) excitation via rotational coupling among molecular orbitals (MO's) at small internuclear distances (e.g., $2p\pi$-$2p\pi$-$2p\sigma$ rotational coupling);

(iii) ionization of molecular orbitals (MO's) via direct coupling to the continuum at small internuclear distances (e.g., $1s\sigma$ ionization).

Briggs[3] showed that, for very slow collisions, direct ionization of MO's [process (iii)] can be explained as the Coulomb ionization from MO's by the slow passage of both nuclei. This process can be described by a first-order Born approximation in the united-atom wave-function basis. For fast collisions, this process can be described by a first-order Born approximation again, but now based upon separated-atom (SA) wave functions. For asymmetric collisions where $Z_1/Z_2 \ll 1$ and $v_1/v_{2K} \geq 1$, direct Coulomb ionization of SA orbitals dominates the ionization process. In the following text we use the notation "Pauli excitation" for both process (i) and process (ii), and use the notation "MO Coulomb ionization" for process (iii).

The region of validity for first-order theories has been extended to both less asymmetric and slower collisions by taking increased binding, Coulomb deflection, relativistic motion of target electrons, polarization of target atom by the incident ion, and energy loss during the collision into

account. Among the easily calculable theories for direct Coulomb ionization, the perturbed stationary-state theory (PSS) taking also the mentioned corrections into account, the ECPSSR theory of Brandt and Lapicki,[4] provides the best overall agreement.[5] However, at low velocities the ECPSSR overpredicts substantially the experiments[6] and the amount of these deviations increases with Z_1/Z_2 for fixed v_1/v_{2K}.

In order to take direct ionization of molecular orbitals in the low-velocity region into account, we recently proposed[7,8] two modifications of the ECPSSR theory (MECPSSR):

(a) The effect of the projectile on the target K electron is not only taken into account by an increased binding energy (binding effect in the ECPSSR), but also by an increased electron velocity, which corresponds to the formation of molecular orbitals for slow projectile velocities. This increase of velocity considerably moderates the effect of binding correction. For very low v_1/v_{2K} the probability for formation of molecular orbitals is effectively reduced by Coulomb deflection.

(b) The effect of Coulomb deflection upon the relativistic correction is taken into account.

The aim of this work is to study K-shell ionization for slow collisions ($0.08 \leq v_1/v_{2K} \leq 0.33$), going from asymmetric ($Z_1/Z_2=0.19$) to less asymmetric ($Z_1/Z_2=0.43$) collisions. For carbon ions on Si, P, S, K, and Ga, no measurements are available in literature (see Ref. 5). For carbon ions on Ca x-ray production, cross-section measurements exist,[9] but they do not cover our low-energy range. To check our procedure, we also measured cross sections for protons, where reliable data already exist (see Ref. 5). The most important results of this work were given recently in a short communication;[10] now all results are given in full detail.

II. EXPERIMENT

We measured simultaneously the x-ray spectra and the spectra of backscattered particles and normalized the x-ray yield to the yield of backscattered particles using elastic-scattering cross sections. The experimental setup is similar to that described before.[6] Here we mention only details which differ from those of Ref. 6.

A 5SDH tandem accelerator at Linz provided carbon ions of 1.0–6.4 MeV with charge states of 1+–3+ and protons of 1 and 2 MeV. The energy of the ion beam was determined by means of a 90° analyzing magnet which was calibrated with an accuracy of 0.3% in energy using the $^{19}F(p,\alpha\gamma)^{16}O$ resonances and a method[11] that is based on the spectrometry of recoil protons produced by elastic scattering of carbon ions in a hydrogen-containing carbon foil. The ion beam was collimated by a stainless-steel aperture 2.4 mm in diameter, mounted 8 cm from the target.

For targets we evaporated thin films of Si, GaP, ZnS, KF, and CaF_2 onto carbon backings. The backings for CaF_2 were polished slices of vitreous carbon. For the other targets we used thin (~ 15 $\mu g/cm^2$) self-supporting carbon foils in order to minimize background in the x-ray region of interest. For every run we used new targets. Virgin targets of KF contained water. We expelled this water before our measurements using ion beams of high current density which were scanned over the targets. The efficiency of this "expulsion procedure" could be seen in the backscattering spectra: "good" targets had a peak-to-background ratio of about 150 for the low-energy side of the potassium backscattering peak. Two sets of targets were used, vanishingly thin and thick enough for ions to attain charge-state equilibrium. The respective thicknesses are listed in Table I, together with the energy loss of carbon ions within the charge-state-equilibrium targets.

The energy resolution of the Si(Li) detector was 180 eV for the Mn $K\alpha$ line. An absorber foil was used between the target and detector in order to attenuate the L x rays and to prevent backscattered energetic ions from reaching the detector. The thickness of our absorber foil was calculated from absorption factors which were measured for the K x rays of our targets. For the evaluation of our spectra, we used the intrinsic photopeak efficiency ϵ_p which was obtained as a product of x-ray-absorption efficiency[12]

$$\epsilon_\alpha = \exp(-\mu_{Be}t_{Be})\exp(-\mu_{Au}t_{Au})[1-\exp(\mu_{Si}t_{Si})] \quad (1)$$

and of the ratio r of photopeak counts to the total counts, (extrapolated to channel zero). Here μ and t are absorption coefficients and thicknesses of the beryllium window, gold front contact, and silicon layer, respectively. The ratio r depends on the x-ray energy and was determined before.[12] The absorption efficiency of the Si(Li) detector

TABLE I. Target thicknesses used for x-ray production cross-section measurements: vanishingly thin targets (t_v), minimum and maximum values for charge equilibrium targets (t_{min}, t_{max}), the upper limit for the characteristic target thickness for our geometry ($t_c \cos\psi$), and minimum, maximum, and typical energy loss of carbon ions within charge equilibrium targets ($\Delta E_{min}, \Delta E_{max}, \Delta E_{typ}$). Thicknesses are given in $\mu g/cm^2$, energy losses are given in keV, and $\psi = 39°$ is the projectile incidence angle with respect to the target surface normal.

Target	t_v	t_{min}	t_{max}	$t_c \cos\psi$	ΔE_{min}	ΔE_{max}	ΔE_{typ}
Si	1.1	25	35	3.2	110	231	205
GaP	1.4	21	33	5.7	56	104	80
ZnS	1.5	15	29	5.6	56	98	75
KF		16	37	3.4	88	200	130
CaF_2	1.1	14	20	3.0	108	147	125

TABLE II. Sources of uncertainties in the measured x-ray cross sections.

(a) Individual systematic errors

	Source	Error (%)
X-rays	Solid angle	1–2
	Intrinsic photopeak efficiency	3–6
	Foil absorption	0.5–2
Particles	Solid angle	1–2
	Backscattering angle	0.5
	Bombarding energy	0.3

(b) Total systematic errors

Si	P	S	K	Ca	Zn	Ga
7%	6%	6%	5%	5%	4%	4%

(c) Nonsystematic errors

Source	Error (%)
X-ray yield[a]	0.5–12
Particle yield[a]	0.5–14, (20)[b]
Pileup and deadtime correction	0.1–0.5
Energy loss within the target[c]	0.5–7

[a]The yield errors are the sum of statistical errors and estimated fit errors.
[b]Upper limit for the uncertainty of the particle yield of potassium.
[c]The energy errors were converted to x-ray cross-section errors using theoretical cross sections for ionization (Ref. 4) and scattering (Ref. 16).

was determined by measuring proton-induced x-ray yield simultaneously with both the Si(Li) detector and the surface barrier detector, which was calibrated[13] using the method proposed earlier.[14] Foil absorption and photopeak efficiency were determined for every individual carbon-ion impact energy, since the energies of K x-rays induced by carbon-ion impact are shifted to higher energies due to multiple ionization. Energies and areas of the photopeaks were determined using the program[15] which fits Gaussian peak shapes and exponential and/or polynomial background to the experimental x-ray spectra.

The number of backscattered ions and the energy loss of ions within the target were determined assuming a linear background due to multiple scattering.

Table II shows the estimated errors in the measured x-ray cross sections.

III. X-RAY PRODUCTION CROSS SECTIONS

The x-ray production cross sections were determined using an iterative evaluation procedure described before.[6]

A. X-ray production by protons

The results are given in Table III. We want to stress that we used scattering cross sections corrected for atomic screening effects following the prescription of Andersen *et al.*,[16] who claim an error smaller than 1%. For protons on light elements, however, nuclear resonances at large proton scattering angles have been observed[17–19] which influence the cross section. For proton energies below 3 MeV, however, data on elastic-scattering cross sections are rare. For proton energies of interest, some data for Si, P, and K are available.[20–22] Unfortunately, we were not able to renormalize our cross sections according to these data since we used a different scattering angle, but a "worst-case normalization uncertainty" of our proton results can be estimated from these data. This normalization uncertainty is at most 10%. The errors given in Table III do not include this normalization error.

TABLE III. Experimental x-ray production cross sections for protons in units of barns. The errors, given in percent below the values for the cross sections, do not include normalization errors due to deviations of proton scattering cross sections from the screened Rutherford scattering cross section (Ref. 16) (see text).

E (MeV)	Si	P	S	K	Ca	Zn	Ga
2.0	917	794	648	357	281	33.7	26.0
	(7%)	(6%)	(6%)	(6%)	(7%)	(5%)	(5%)
1.0	546	381	298	130	95.4	5.48	4.12
	(7%)	(6%)	(6%)	(6%)	(7%)	(5%)	(5%)

B. X-ray production by carbon ions

It is well known[23–26] that x-ray production cross sections may depend on the charge state of the bombarding ions. In cases where projectiles carry one or two K-shell holes, a significant cross-section enhancement due to electron capture is observed, but only small effects are found for projectiles with filled K-shell but different L-shell vacancy configurations. The charge state of incoming carbon ions was always $Q_0 \leq 3+$ in this work. But because we did not have single collision conditions (infinitely thin targets, see Table I), we had also charge states $Q > Q_0$ within our targets. Figure 1 shows the experimental equilibrium charge state of carbon ions for different target materials taken from Wittkower and Betz.[27] As can be seen, the equilibrium charge state Q_m is larger than $3+$ for carbon ion energies $E > 2.5$ MeV, independent of target material. To examine the influence of projectile charge on the x-ray-production cross section (σ^x) we measured σ^x for several carbon-ion energies on silicon and CaF_2 for different target thicknesses. The results are given in Fig. 2 where we plotted normalized x-ray production cross sections σ_n versus target thickness, measured along the beam direction. For Si, the x-ray production cross sections for infinitely thick targets are enhanced by a factor of 1.4 and for CaF_2 up to 1.15, compared to those for vanishingly thin targets. As the thickness effect is larger for lighter targets than for heavier ones, these two values should provide an upper and lower limit for the importance of the effect. However, we want now to discuss this more quantitatively. The ions penetrating the target attain their equilibrium charge state exponentially with target depth. We can therefore easily determine the characteristic target thickness t_c for attaining the equilibrium charge state by fitting the function $a - b(1-\exp(-t/t_c))t_c/t$ (Eq. 5.5.26 of Ref. 28, note an error there) to the data of Fig. 2. The results of the fit varied between $t_c = 1.5$–4.1 μg/cm^2. These values will now be compared to the values for the characteristic targets thickness given by the following theories:

(a) In an early work, Brandt *et al.*[29] proposed t_c to be

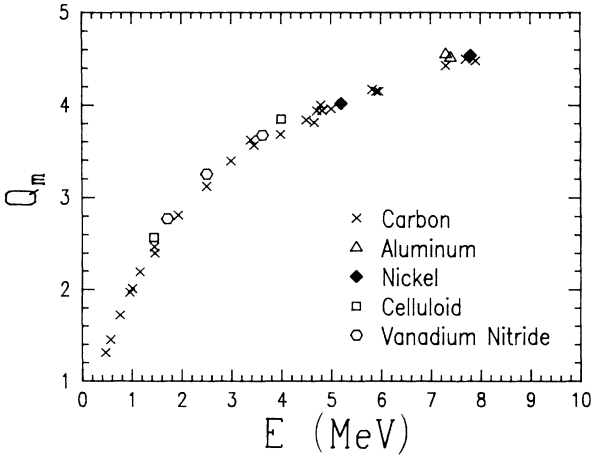

FIG. 1. Mean charge Q_m of carbon ions behind solids.

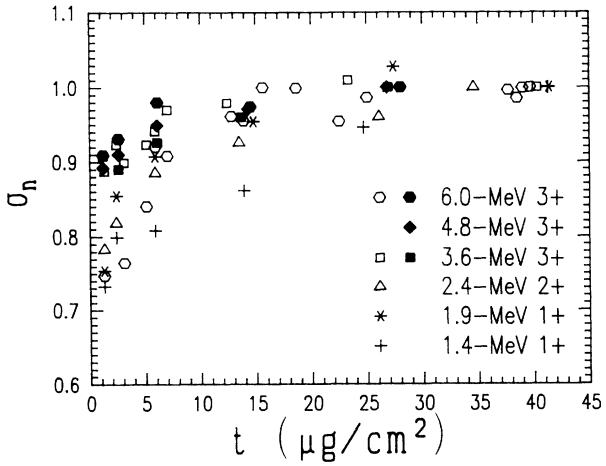

FIG. 2. X-ray production cross sections σ_n normalized to the values for the thickest targets as a function of the target thickness (measured in the beam direction). Open and closed symbols are used for Si and CaF_2, respectively.

equal to v_1/λ, where v_1 is the projectile velocity and λ is the dynamic screening rate, proportional to the plasma frequency of the free electron gas: $\lambda \approx \omega_p/42$. Though this model was criticized by Gray *et al.*,[30] it gives for 6-MeV carbon ions a reasonable value of $t_c = 3.9$ μg/cm^{-2}.

(b) According to Betz *et al.*,[31] the projectile beam is decomposed into two components, one with and the other without the K-shell vacancies. Since the charge-state distribution in the target is approximately known,[27] we can use Eq. (2) of Ref. 31 and express the characteristic target thickness as

$$t_c = \frac{(1-j_\infty)v_1\tau}{1+n\sigma_c v_1\tau} . \tag{2}$$

Here j_∞ is the fraction of the beam having at least one K-shell vacancy in an infinitely thick target, v_1 is the projectile velocity, τ is the K-shell vacancy quenching time due to radiative and Auger processes, n is the density of target atoms, and σ_c is the cross section for the electron capture into the projectile K shell. Using σ_c from Ref. 32 and $\tau \approx 10^{-14}$ s (see Ref. 33), $n\sigma_c v_1\tau$ is small compared to unity and can be neglected. The characteristic target thickness (2) therefore essentially depends on τ. For Ne projectiles, Groeneveld *et al.*[34] found good agreement between his fitted value of τ and the experimental one of Mehlhorn[35] for the K-vacancy quenching time in gaseous Ne. The theoretical τ value of McGuire[33] is higher by a factor of 2.7 than the experimental one.[35] Since for carbon ions the experimental values for τ are not available, we have used the theoretical calculation according to McGuire[33] which we corrected simply by multiplying it by the ratio of the experimental[35] to theoretical[33] value for Ne. With $\tau = 3.8 \times 10^{-15}$ s so obtained and j_∞ estimated from Ref. 27, the values for t_c varied between 4.2 and 6.9 μg/cm^{-2} for carbon ions of 1.4–6 MeV which is above our fitted values by a factor of 2. We shall then

generalize this result to other targets. As j_∞, v_1, and τ (or v_1 and approximately λ according to Brandt[29]) are all target independent, we expect the same for t_c. However, as our thicknesses are given in $\mu g/cm^2$, t_c depends on target density only. The cross sections measured for target thicknesses greater than several t_c are hence equilibrium cross sections independent of target thickness. Target thicknesses $t \lesssim t_c/3$ can be regarded as vanishingly thin and the cross sections measured are those of ions having the incoming charge state.

Table I shows the values of our vanishingly thin targets (t_v) and the range of target thicknesses used for the equilibrium x-ray production cross-section measurements together with the energy loss of carbon ions within those targets. We also show in Table I the upper limit for the characteristic target thickness t_c multiplied by $\cos\psi$, where ψ is the projectile incidence angle ($\psi = 39°$). For the elements other than Si and Ca we have scaled our experimental value of t_c with the corresponding density ratio. As can be seen from Table I, the target thicknesses used were either smaller than $t_c(\cos\psi)/3$ or larger than $3t_c\cos\psi$, except for a few cases of sulfur. The results given in Table IV are hence x-ray production cross sections for carbon ions having the incoming charge state Q_0 within the target. The results given in Table V are equilibrium x-ray production cross sections and include all possible ionization mechanisms. For convenience we give in Table IV also the ratios of equilibrium x-ray production cross section and x-ray production cross section for vanishingly thin targets. As can be seen, the ratios are close to unity except for phosphorus and silicon, where the equilibrium x-ray production cross section are up to 35% higher than cross sections for vanishingly thin targets.

IV. DISCUSSION

A. K-shell ionization by protons

We used fluorescence yields of Krause[36] to convert our x-ray production cross sections to ionization cross sec-

TABLE IV. Experimental x-ray production cross sections for carbon ions on vanishingly thin targets given in barns. Experimental errors are given in percent below the values. The ratios of the cross section for charge equilibrium and vanishingly thin targets are given in square brackets. The charge state of incoming ions was 1+ for $E < 3$ MeV and 3+ for $E > 4.8$ MeV.

E (MeV)	Si	P	S	Ca	Zn	Ga
6.4	248×10^1 (12%) [1.30]	128×10^1 (12%) [1.26]	729.0 (12%) [1.13]	87.7 (10%) [1.13]	4.23 (10%) [1.01]	3.34 (10%) [0.95]
5.6	138×10^1 (12%) [1.28]	695.0 (12%) [1.23]	409.0 (12%) [1.06]	51.7 (11%) [1.08]	2.53 (12%) [1.04]	2.11 (12%) [1.03]
4.8	752.0 (13%) [1.14]	377.0 (13%) [1.08]	196.0 (13%) [1.06]	28.1 (12%) [1.09]	1.50 (14%) [1.03]	1.17 (14%) [0.95]
4.2	396.0 (14%) [1.19]	196.0 (14%) [1.17]	124.0 (14%) [0.99]	16.1 (14%) [1.14]	8.55×10^{-1} (16%) [1.00]	6.24×10^{-1} (16%) [0.98]
3.6	218.0 (14%) [1.19]	109.0 (15%) [1.14]	62.9 (16%) [0.96]	8.80 (16%) [1.09]	5.43×10^{-1} (18%) [0.99]	3.43×10^{-1} (18%) [1.04]
3.0	102.0 (15%) [1.30]	52.2 (16%) [1.16]	28.0 (17%) [1.06]	4.25 (18%) [1.11]	1.72×10^{-1} (18%) [1.36]	1.31×10^{-1} (20%) [1.18]
2.4	39.6 (15%) [1.33]	17.5 (20%) [1.25]	9.10 (20%) [1.11]	1.83 (20%) [1.04]	1.00×10^{-1} (20%) [0.77]	
1.9	13.4 (16%) [1.34]	7.02 (25%) [0.97]	3.15 (25%) [1.11]	6.74×10^{-1} (25%) [1.43]		
1.4	3.24 (20%) [1.44]					
1.2	2.17 (20%) [1.10]					

TABLE V. Experimental equilibrium x-ray production cross sections for carbon ions on various targets given in barns. Experimental errors are given in percent below the values. The charge state of incoming carbon ions was 1+ for $E < 3$ MeV and 3+ for $E > 4.8$ MeV.

E (MeV)	Si	P	S	K	Ca	Zn	Ga
6.4	322×10^{1} (9%)	161×10^{1} (9%)	822 (8%)	151 (7%)	98.9 (6%)	4.26 (6%)	3.17 (6%)
6	238×10^{1} (9%)	118×10^{1} (9%)	586 (8%)	112 (7%)	74.4 (6%)	3.43 (6%)	2.59 (7%)
5.6	176×10^{1} (9%)	856 (10%)	434 (9%)	84.5 (8%)	55.8 (6%)	2.63 (7%)	2.18 (7%)
5.2	125×10^{1} (9%)	615 (10%)	306 (9%)	63.7 (9%)	42.9 (7%)	2.08 (7%)	1.57 (7%)
4.8	856 (10%)	407 (10%)	208 (9%)	48.4 (11%)	30.6 (7%)	1.54 (8%)	1.11 (8%)
4.5	651 (10%)	326 (10%)	164 (10%)	33.8 (12%)	25.1 (7%)	1.20 (8%)	9.72×10^{-1} (8%)
4.2	472 (10%)	229 (10%)	123 (10%)	26.1 (12%)	18.4 (8%)	8.58×10^{-1} (9%)	6.09×10^{-1} (9%)
3.9	357 (10%)	166 (11%)	85.5 (10%)	18.4 (12%)	13.1 (8%)	6.40×10^{-1} (9%)	4.81×10^{-1} (9%)
3.6	259 (10%)	124 (11%)	60.5 (10%)	12.8 (14%)	9.55 (8%)	5.35×10^{-1} (9%)	3.56×10^{-1} (9%)
3.3	187 (10%)	85.9 (12%)	44.1 (11%)	9.36 (15%)	6.68 (9%)	3.37×10^{-1} (10%)	2.38×10^{-1} (10%)
3.0	133 (10%)	60.7 (12%)	29.8 (11%)	6.28 (15%)	4.72 (9%)	2.34×10^{-1} (10%)	1.55×10^{-1} (10%)
2.8	101 (11%)	44.6 (13%)	21.4 (11%)	4.60 (16%)	3.62 (9%)	1.57×10^{-1} (10%)	1.21×10^{-1} (10%)
2.6	76.5 (11%)	31.1 (13%)	14.9 (11%)	3.49 (16%)	2.59 (10%)	1.12×10^{-1} (11%)	7.63×10^{-2} (11%)
2.4	52.5 (12%)	21.8 (14%)	10.1 (11%)	2.64 (16%)	1.90 (10%)	7.65×10^{-2} (11%)	4.64×10^{-2} (11%)
2.2	36.4 (12%)	14.1 (14%)	6.74 (12%)	1.79 (17%)	1.36 (12%)	4.82×10^{-2} (12%)	3.20×10^{-2} (12%)
2	22.8 (13%)	8.59 (15%)	4.30 (12%)	1.16 (17%)	9.26×10^{-1} (13%)	3.30×10^{-2} (13%)	1.82×10^{-2} (13%)
1.9	18.0 (13%)	6.84 (15%)	3.49 (13%)	9.61×10^{-1} (20%)	7.44×10^{-1} (13%)	2.24×10^{-2} (14%)	1.65×10^{-2} (14%)
1.8	14.0 (14%)	5.17 (16%)	2.85 (13%)	8.05×10^{-1} (17%)	6.01×10^{-1} (14%)	1.63×10^{-2} (15%)	1.03×10^{-2} (15%)
1.7	11.1 (15%)	3.98 (17%)	2.17 (14%)	6.15×10^{-1} (17%)	4.75×10^{-1} (14%)		
1.6	8.17 (15%)	2.99 (17%)	1.75 (14%)	4.79×10^{-1} (20%)	3.54×10^{-1} (14%)		
1.5	6.09 (16%)	2.41 (17%)	1.28 (15%)	3.67×10^{-1} (20%)	2.69×10^{-1} (15%)		
1.4	4.66 (17%)	1.84 (18%)	9.80×10^{-1} (15%)	3.25×10^{-1} (22%)	2.00×10^{-1} (15%)		
1.3	3.44 (17%)	1.33 (18%)	7.84×10^{-1} (16%)	2.10×10^{-1} (22%)	1.32×10^{-1} (15%)		

TABLE V. (*Continued*).

E (MeV)	Si	P	S	K	Ca	Zn	Ga
1.2	2.39 (18%)	9.59×10^{-1} (18%)	5.12×10^{-1} (16%)	1.41×10^{-1} (23%)	8.59×10^{-2} (15%)		
1.1	1.68 (18%)	6.88×10^{-1} (19%)	3.58×10^{-1} (17%)	8.48×10^{-2} (25%)	5.38×10^{-2} (15%)		
1	1.09 (18%)	5.75×10^{-1} (20%)	2.38×10^{-1} (17%)	4.96×10^{-2} (25%)	3.17×10^{-2} (15%)		

tions. The ionization cross sections were then compared to the empirical reference cross sections σ_r given by Paul[37] and to theoretical cross sections given below.

(a) Brandt and Lapicki,[4] who calculated plane-wave Born-approximation cross sections corrected for binding, polarization, energy loss during collision, Coulomb, and relativistic effects (σ_{ECPSSR}, direct ionization only).

(b) Laegsgaard, Andersen, and Lund,[38] who calculated semiclassical approximation cross sections corrected for binding, Coulomb, and relativistic effects (σ_{SCA}).

(c) Montenegro and Sigaud[39] (MS), who apply adiabatic perturbation theory to the ionization of $1s\sigma$ molecular orbital by direct Coulomb interaction in asymmetric ion atom collisions and extend the theory to less adiabatic collisions by imposing an asymptotic matching with the semiclassical approximation (σ_{MS}). To make comparisons to theory more convenient we show in Table VI our experimental ionization cross sections (σ_{expt}) normalized to the reference cross sections[37] ($S_r=\sigma_{\mathrm{expt}}/\sigma_r$), the ECPSSR cross sections[4] ($S_e=\sigma_{\mathrm{expt}}/\sigma_{\mathrm{ECPSSR}}$), the SCA cross sections[38] ($S_s=\sigma_{\mathrm{expt}}/\sigma_{\mathrm{SCA}}$), and the cross sections by Montenegro and Sigaud[39] ($S_m=\sigma_{\mathrm{expt}}/\sigma_{\mathrm{MS}}$), respectively. Proton energy is given in MeV and the scaled projectile velocity is given by $\xi=2v_1/(\Theta v_{2K})$, where v_1 is the lab projectile velocity, v_{2K} is the hydrogenic velocity of the target K electron, and $\Theta=I_K/(Z_2-0.3)^2R$, with I_K being the experimental ionization energy and R the Rydberg energy. We want to note that ECPSSR and MECPSSR predict identical cross sections in the ξ range considered. We therefore omitted comparisons with MECPSSR. As can be seen from the values for S_r, our experimental cross sections are in good agreement with the reference cross sections[37] (well within the combined errors of our values and of the reference cross sections), with exception of the 1-MeV value of Si and the 2-MeV values of K and Ca, which deviate from unity by slightly more than the stated experimental error. These deviations probably occur due to resonances in the elastic-scattering cross esctions. The ECPSSR predictions[4] are in good agreement with our experiment. The MS predictions[39] are slightly worse. The SCA theory[38] is much too low for high ξ, since its binding correction[40] is not valid for $\xi>0.25$.

B. *K*-shell ionization by carbon ions

For comparison with the theories we shall use our charge-state equilibrium cross sections, since Table V is more complete than Table IV and the experimental errors are smaller. Further, the difference between both sets of cross sections will be shown to be smaller than the difference between theoretical and experimental cross sections.

We used a procedure described in detail before[6] to estimate the enhancement of the K-shell fluorescence yield ω due to multiple outer-shell ionization from the measured energy shifts of the K x-rays. For Si, P, and S we estimated ω from the $K\alpha$ line shift only, since we were not able to determine K_β line shifts and intensity ratios of K_β and K_α lines (I_β/I_α) accurately enough. As a result of these calculations we plotted in Fig. 3 the ratios ω/ω_0 as a function of the scaled velocity ξ. Here ω_0 is the fluorescence yield of singly ionized target atoms which we have taken from Krause.[36] The deviation from unity is significant for the highest carbon-ion velocities. We used the enhanced fluorescence yields to convert our x-ray production cross sections for Si, P, S, K, and Ca into ionization cross sections. For Zn and Ga, however, the effect of multiple outer-shell ionization on the fluorescence yield is small, hence we used Krauses[36] values.

Figures 4–7 show our experimental equilibrium ionization cross sections normalized to the same theoretical predictions for Coulomb ionization as for proton impact, as a function of the scaled velocity ξ. The ECPSSR

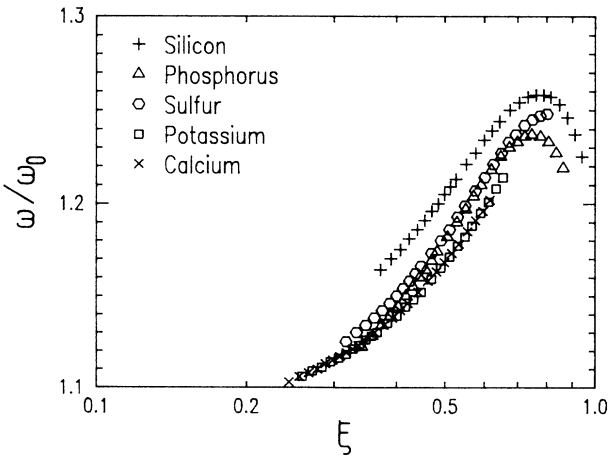

FIG. 3. Ratios of K-shell fluoresence yields ω for multiple ionized targets to fluorescence yields for single ionized targets ω_0 versus scaled carbon projectile velocity.

TABLE VI. Experimental ionization cross sections for protons on various targets (atomic number Z_2) normalized to reference cross sections (S_r), ECPSSR cross sections (S_e), SCA cross sections (S_s) and $1s\sigma$-MO-Coulomb ionization cross sections (S_m). Proton energy is given in MeV.

E (MeV)	Z_2	ξ	S_r	S_e	S_s	S_m
2.0	14	1.81	0.98	1.03	1.72	1.09
2.0	15	1.67	1.01	1.05	1.64	1.11
2.0	16	1.55	0.95	0.98	1.46	1.05
2.0	19	1.26	0.92	0.93	1.22	1.00
2.0	20	1.19	0.90	0.91	1.14	0.97
2.0	30	0.75	1.00	0.97	0.96	0.99
2.0	31	0.72	0.97	0.94	0.92	0.96
1.0	14	1.28	1.11	1.12	1.64	1.23
1.0	15	1.18	1.03	1.03	1.39	1.11
1.0	16	1.09	1.03	1.02	1.31	1.10
1.0	19	0.89	1.05	1.03	1.16	1.07
1.0	20	0.84	1.03	1.02	1.10	1.04
1.0	30	0.53	1.04	0.99	0.88	0.95
1.0	31	0.51	1.02	0.98	0.87	0.93

theory (Fig. 4) which predicts direct Coulomb ionization well for small ratios Z_1/Z_2 and for high velocities[5] cannot reproduce the experimental data at low projectile velocities and becomes worse with increasing Z_1/Z_2. The SCA predictions (Fig. 5) show a reverse behavior. The SCA fails at high velocities but predicts experimental results well at low velocities. The predictions of Montenegro and Sigaud (Fig. 6) deviate in all ξ ranges from the experimental data. Figure 7 shows the ionization cross sections normalized to our MECPSSR theory.[7,8] Here for both, low and high ξ values the experiment and theory agree quite well, except for the hump centered at $\xi \sim 0.6$, which increases with increasing Z_1/Z_2.

As we mentioned above, in our equilibrium x-ray production cross section measurements we had charge states $Q > Q_0$ within the targets and hence target K-to-projectile K' electron capture[32] could contribute to our measured cross sections. We calculated the possible electron-transfer contributions using a procedure described in detail before.[6] The result is given in Fig. 8, where we plotted the calculated enhancement factor F due to K-to-S' electron transfer versus ξ. For high ion energies the enhancement factor due to K-to-S' electron capture agrees well with the ratios of x-ray production cross sections for charge-state equilibrium and vanishingly thin targets, given in Table IV. The ratios for low ion energies cannot be explained fully by K-to-S' electron capture. However, it is also obvious that K-to-S' electron capture cannot explain the hump in Fig. 7.

It is known[41–43] that for $Z_1/Z_2 \geq 0.3$ and $v_1/v_{2K} < 1$ Pauli excitation can contribute significantly to K-shell ionization. To calculate the cross section for the ionization of the $1s\sigma$ orbital we used a statistical treatment of the electron promotion from inner shells into the continuum.[44–46] We first calculated the sum of K-shell ionization cross sections for the projectile and target atom us-

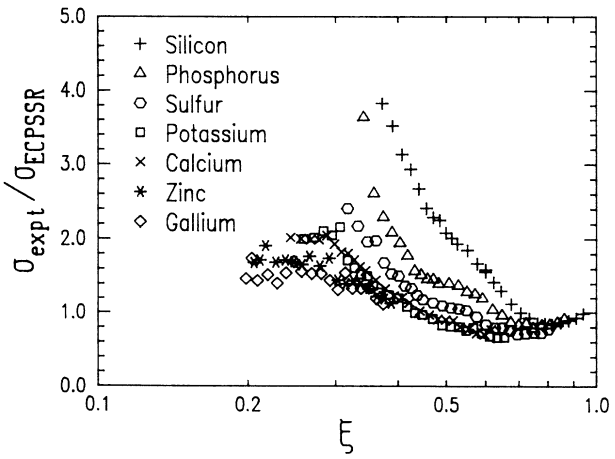

FIG. 4. Experimental equilibrium ionization cross sections σ_{expt} normalized to ECPSSR cross sections σ_{ECPSSR}.

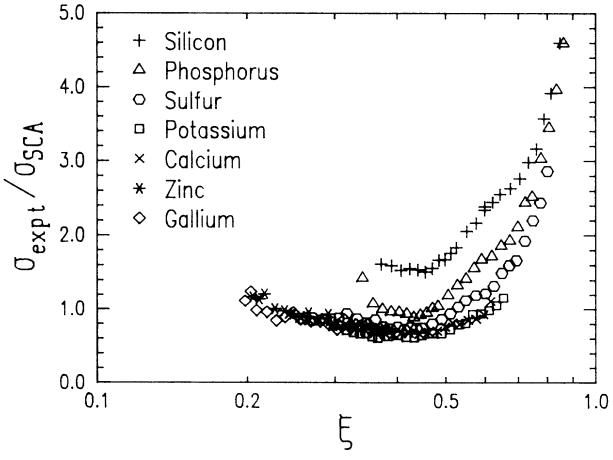

FIG. 5. Experimental equilibrium ionization cross sections σ_{expt} normalized to SCA cross sections σ_{SCA}.

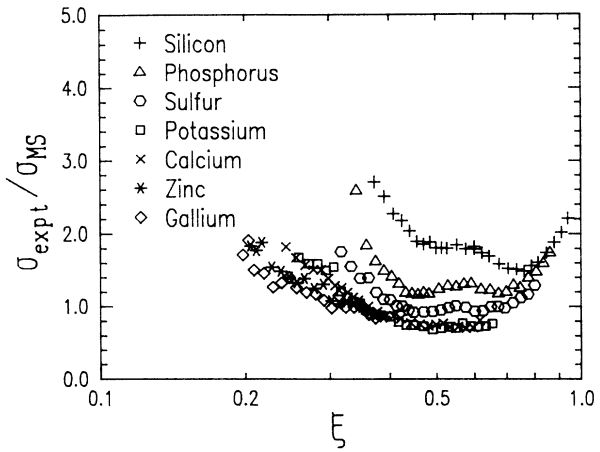

FIG. 6. Experimental equilibrium ionization cross sections σ_{expt} normalized to predictions of Montenegro and Sigaud σ_{MS}.

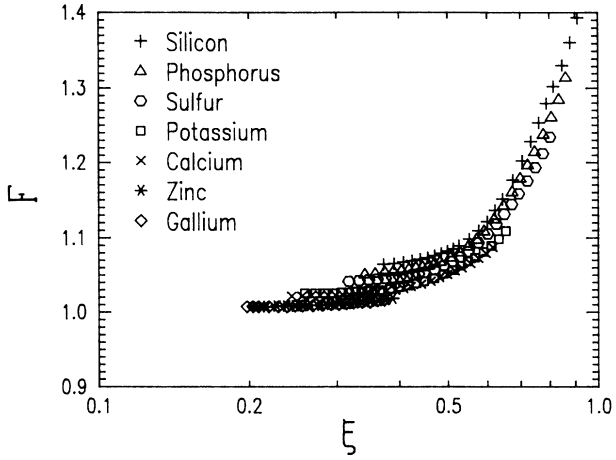

FIG. 8. Calculated enhancement factor F due to K-to-S'-shell electron capture for our targets.

ing the diffusion model of Mittelman and Wilets[44] σ_{MW} and the diffusion constants for Brandt.[46] Then the K-shell ionization cross section of the target atoms was found by multiplying the summed cross section by the vacancy-sharing factor (V) of Meyerhof *et al.*[47] However, we calculated V using the K-shell binding energy (E_B) for the carbon ions, which depends on the charge state Q within the targets, rather than the neutral-atom binding energy.

We simply used $E_B(Z_1,Q)=Z_1^2R$ for $Z_1-Q\leq 1$ and $E_B(Z_1,Q)=(Z_1-0.3-nq)^2R$ for $Z_1-Q>1$, where $Z_1=6$, R is the Rydberg energy, $n=Z_1-Q-2$ is the number of L electrons and q is determined by the neutral-atom binding energy.[48] Since the ions within the target have a charge-state distribution[27] of width D and mean charge Q_m, we calculated the normalized distribution function of charge states $P(Q_m,D,Q)$ and obtained finally our vacancy sharing factor $V(Q_m,D)=\sum_{Q=0}^{Z_1}P(Q_m,D,Q)V(Q)$. We used a Guassian charge-state distribution for $P(Q_m,D,Q)$, and the values for Q_m and D were obtained from the least-squares fit of a polynomial to the corresponding experimental values given by Wittkower and Betz.[27]

Figure 9 shows the experimental equilibrium ionization cross section normalized to the diffusion cross section (σ_{MW}) thus calculated. It can be seen that Pauli excitation gives the largest contributions for $\xi\sim 0.6$ where we had the largest discrepancies in Fig. 7. For lower projectile velocities, Pauli excitation decreases obviously more quickly than direct MO-Coulomb ionization, mainly due to the strong dependence of the vacancy sharing factor upon ion velocity. For higher velocities, direct Coulomb ionization increases faster than Pauli excitation.

We want to note that we also calculated the cross sections for the direct $2p\pi$-$2p\sigma$ rotational coupling with the subsequent target K-shell ionization for projectiles having $2p$ vacancies produced during earlier collisions in the target.[47,49] but the cross sections were lower by a factor of 3

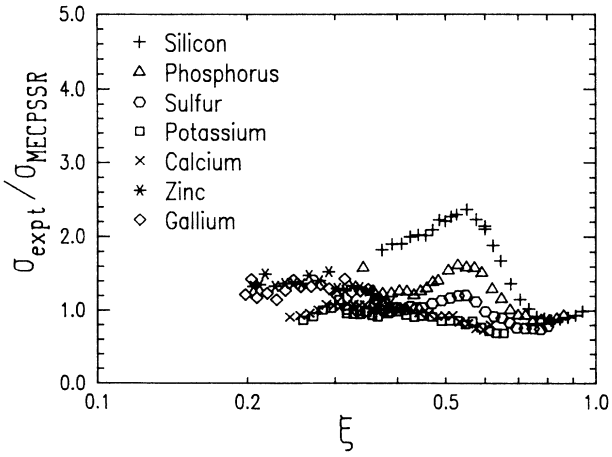

FIG. 7. Experimental equilibrium ionization cross sections σ_{expt} normalized to MECPSSR cross sections $\sigma_{MECPSSR}$.

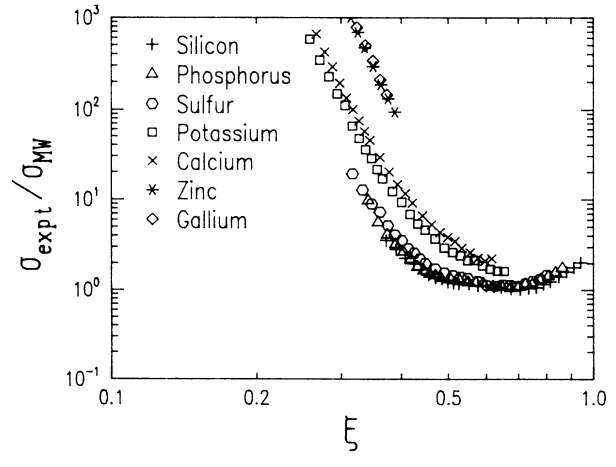

FIG. 9. Experimental equilibrium ionization cross sections σ_{expt} normalized to diffusion cross sections σ_{MW}.

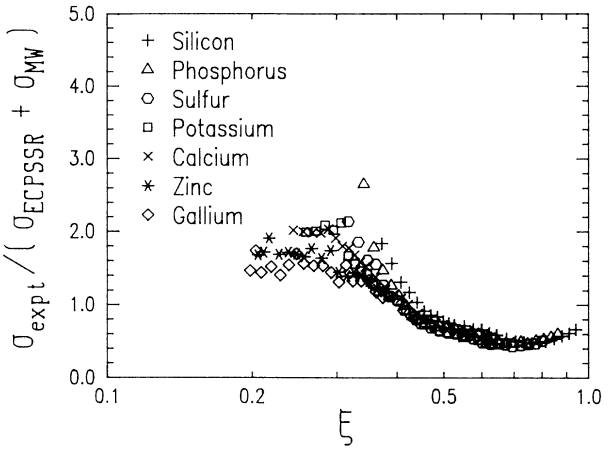

FIG. 10. Experimental equilibrium ionization cross sections σ_{expt} normalized to the sum of ECPSSR cross sections σ_{ECPSSR} and diffusion cross sections σ_{MW}.

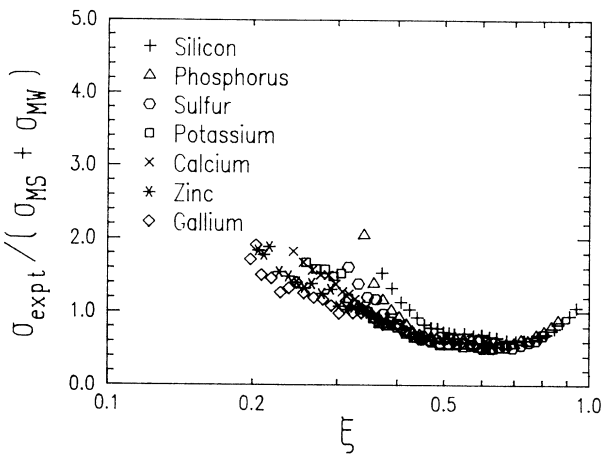

FIG. 12. Experimental equilibrium ionization cross sections σ_{expt} normalized to the sum of the cross sections of Montenegro and Sigaud σ_{MS} and diffusion cross sections σ_{MW}.

than the values from the diffusion model and hence too small to explain the hump in Fig. 6. This may be due to the fact that projectile K vacancies were not considered.

In Figs. 10–13 we show now the experimental equilibrium cross sections normalized to the sum of the predictions for direct Coulomb excitation and Pauli excitation. We did not include the electron capture[32] explicitly because we included Pauli excitation. Here the semiempirical diffusion constant[46] was used, which was obtained with no distinction between the vanishingly thin and charge-state equilibrium targets. The prediction agree now much better with the experiments. The steep increase for $\xi > 0.5$ in Fig. 5 (SCA prediction) is strongly reduced (see Fig. 11) and the significant maximum in Fig. 7 at $\xi \sim 0.6$ (MECPSSR predictions) has completely disappeared (see Fig. 13). The remaining deviations from unity have been reduced to 50%. We assume that these deviations might be due to uncertainties in the fluorescence yields used (see Fig. 3) and the uncertainty in the semiempirical diffusion constant which might also depend on the charge state of the ions. This assumption is further supported by the difference between the cross sections for vanishingly thin and charge-state equilibrium targets, which does not disappear for low carbon-ion energies (see ratios given in Table IV). Within these uncertainties, we now obtain good agreement between the experimental results and theory so far as SCA (Fig. 11) and MECPSSR (Fig. 13) are considered which either use an united atom binding correction (SCA) or ionization of molecular orbitals for the very low ξ range (MECPSSR), respectively. ECPSSR predictions (Fig. 10) are too low for $\xi > 0.3$ and the same holds for the predictions of Montenegro and Sigaud (Fig. 12).

V. SUMMARY AND CONCLUSION

Experiental ionization cross sections for protons and carbon ions on Si, P, S, K, Ca, Zn, and Ga were com-

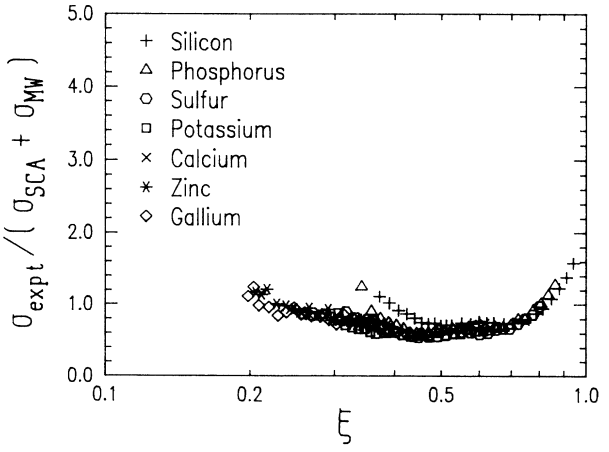

FIG. 11. Experimental equilibrium ionization cross sections σ_{expt} normalized to the sum of SCA cross sections σ_{SCA} and diffusion cross sections σ_{MW}.

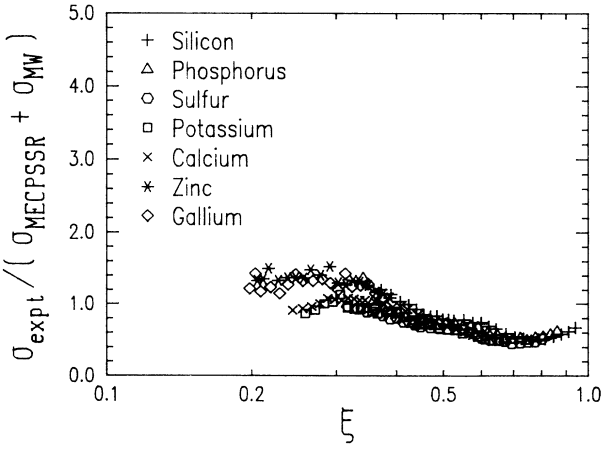

FIG. 13. Experimental equilibrium ionization cross sections σ_{expt} normalized to the sum of MECPSSR cross sections $\sigma_{MECPSSR}$ and diffusion cross sections σ_{MW}.

pared to theoretical predictions for direct Coulomb ionization and Pauli excitation. For protons, good agreement with the reference cross sections and the ECPSSR and MECPSSR predictions was found. For carbon ions we present measurements of ionization cross sections for our targets and $\xi < 1$. We compared our results to the theories for direct Coulomb ionization and for Pauli excitation and found that both $\sigma_{\mathrm{MECPSSR}}+\sigma_{\mathrm{MW}}$ and $\sigma_{\mathrm{SCA}}+\sigma_{\mathrm{MW}}$ predict our experiments best. It is therefore obvious that the direct Coulomb ionization of atomic orbitals, the Pauli excitation via interacting level crossing, and the direct Coulomb ionization again, but now of molecular oritals, are the significant K-shell ionization mechanism for carbon ions on targets with $Z_1/Z_2 \sim 0.4$, for high ion velocities, intermediate velocities, and lowest velocities, respectively.

ACKNOWLEDGMENTS

We would like to thank Professor Helmut Paul for calculating the reference cross sections and for many helpful discussions. One of the authors (Ž.Š.) is indebted to the Johannes-Kepler-University of Linz for kind hospitality and to the Upper Austrian Government for supporting his stay in Linz within the Alps-Adria cooperation program.

[1]D. H. Madison and E. Merzbacher, in *Atomic Inner Shell Processes,* edited by B. Crasemann (Academic, New York, 1975).
[2]U. Wille and R. Hippler, Phys. Rep. **132**, 129 (1986).
[3]J. S. Briggs, J. Phys. B **8**, L485 (1975).
[4]W. Brandt and G. Lapicki, Phys. Rev. A **23**, 1717 (1981).
[5]H. Paul and J. Muhr, Phys. Rep. **135**, 47 (1986).
[6]M. Geretschläger and O. Benka, Phys. Rev. A **34**, 866 (1986).
[7]O. Benka, M. Geretschläger, and H. Paul, J. Phys. (Paris) Colloq. **12**, C9-251 (1987).
[8]O. Benka, M. Geretschläger, and H. Paul (unpublished).
[9]R. M. Wheeler, R. P. Chaturvedi, J. L. Duggan, J. Tricomi, and P. D. Miller, Phys. Rev. A **13**, 958 (1976).
[10]M. Geretschläger, Ž. Šmit, and O. Benka, J. Phys. B **21**, L603 (1988).
[11]S. Blümner and F. Rauch, Nucl. Instrum. Methods **221**, 472 (1984).
[12]M. Geretschläger, Nucl. Instrum. Methods B **28**, 289 (1987).
[13]M. Geretschläger (unpublished).
[14]M. Geretschläger, Nucl. Instrum. Methods **192**, 117 (1982).
[15]E. Steinbauer, Ph.D. thesis, Verband der wissenschafltichen Gesellschaften Österreichs (VWGÖ), A-1070 Wien, 1987.
[16]H. H. Andersen, F. Besenbacher, P. Loftager, and W. Möller, Phys. Rev. A **21**, 1891 (1980).
[17]P. M. Endt and C. Van der Leun, Nucl. Phys. A **310**, 1 (1978).
[18]P. M. Endt and C. Van der Leun, Nucl. Phys. A **214**, 1 (1973).
[19]P. M. Endt and C. Van der Leun, Nucl. Phys. A **105**, 1 (1967).
[20]S. Rubin, L. E. Bailey, and T. O. Passell, Phys. Rev. **114**, 1110 (1959).
[21]G. Guernet, E. Ligeon, N. Longequene, Tsan Ung Chan, and J. P. Longequene, J. Phys. **29**, 9 (1968).
[22]E. Rauhala, Nucl. Instrum Methods B **12**, 447 (1985).
[23]T. J. Gray, in *Methods of Experimental Physics,* edited by P. Richard (Academic, New York, 1980), Vol. 17, p. 250.
[24]B. Knaf, G. Presser, and J. Stähler, Z. Phys. A **282**, 25 (1977).
[25]G. Presser, E. Scherer, and J. Stähler, Z. Phys. A **295**, 27 (1980).
[26]H. Tawara, P. Richard, T. J. Gray, P. Pepmiller, J. R. Macdonald, and R. Dilligham, Phys. Rev. A **19**, 2131 (1979).
[27]A. B. Wittkower and H. D. Betz, At. Data Nucl. Data Tables **5**, 113 (1973).
[28]T. J. Gray, in *Methods of Experimental Physics,* edited by P. Richard (Academic, New York, 1980), Vol. 17, p. 264.
[29]W. Brandt, R. Laubert, M. Mourino, and A. Schwarzschild, Phys. Rev. Lett. **30**, 358 (1973).
[30]T. J. Gray, P. Richard, K. A. Jamison, J. M. Hall, and R. K. Gardner, Phys. Rev. A **14**, 1333 (1975).
[31]H. D. Betz, F. Bell, H. Panke, G. Kalkoffen, M. Welz, and D. Evers, Phys. Rev. Lett. **33**, 807 (1974).
[32]G. Lapicki and F. D. McDaniel, Phys. Rev. A **22**, 1896 (1980).
[33]E. J. McGuire, Phys. Rev. **185**, 185 (1969).
[34]K. O. Groeneveld, B. Kolb, J. Schader, and K. D. Sevier, Z. Phys. A **277**, 13 (1976).
[35]W. Mehlhorn, D. Stalherm, and H. Verbeek, Z. Naturforsch. **23A**, 287 (1968).
[36]M. O. Krause, J. Phys. Chem. Ref. Data **8**, 307 (1979).
[37]H. Paul and J. Sacher, At. Data Nucl. Data Tables **42**, 105 (1989).
[38]E. Laegsgaard, U. J. Andersen, and M. Lund, in *Proceedings of the Tenth International Conference on Physics of Electron and Atomic Collisions, Paris, 1977,* edited by G. Watel (North-Holland, Amsterdam, 1977).
[39]E. C. Mongenegro and G. M. Sigaud, J. Phys. B **18**, 299 (1985).
[40]H. Paul, Nucl. Instrum. Methods **169**, 249 (1980).
[41]U. Fano and W. Lichten, Phys. Rev. Lett. **14**, 627 (1963).
[42]K. Taulbjerg, J. S. Briggs, and J. Vaaben, J. Phys. B **9**, 1351 (1976).
[43]W. E. Meyerhof and K. Taulbjerg, Annu. Rev. Nucl. Sci. **27**, 279 (1977).
[44]M. H. Mittelman and L. Wiltes, Phys. Rev. **154**, 12 (1967).
[45]W. Brandt and K. W. Jones, Phys. Lett. **57A**, 35 (1976).
[46]W. Brandt, IEEE Trans. Nucl. Sci. **NS-26**, 1179 (1979).
[47]W. E. Meyerhof, R. Anholt, and T. K. Saylor, Phys. Rev. A **16**, 169 (1977).
[48]*Tables of Isotopes,* 7th edition, edited by C. M. Lederer and V. S. Shirley (Wiley, New York, 1978).
[49]K. Taulbjerg, S. B. Briggs, and J. Vaaben, J. Phys. B **9**, 1351 (1976).